

The large scale distribution and structure of dark matter halos

Surhud More^{*†}

Kavli Institute for the Physics and Mathematics of the Universe

E-mail: surhud.more@ipmu.jp

Halo assembly bias – the dependence of the large scale clustering amplitude of halos on secondary parameters other than the halo mass – is a well established prediction of the standard structure formation model. However it has been notoriously hard to confirm, observationally. I will review our recent attempts to detect halo assembly bias on cluster scales using a novel combination of weak gravitational lensing and the clustering of galaxy clusters. We have been able to construct two cluster subsamples which share the same mass, but have a different clustering amplitude. I will also present evidence of the splashback radius or the edges of galaxy cluster halos in observations. The splashback radius is sensitive to the current mass accretion rate on to halos. The two cluster subsamples which show halo assembly bias, also display different locations for their splashback radii, establishing that they differ in their current mass accretion rates.

*11th International Workshop Dark Side of the Universe 2015
14-18 December 2015
Yukawa Institute for Theoretical Physics, Kyoto University Japan*

^{*}Speaker.

[†]A footnote may follow.

1. Clustering of dark matter halos

1.1 Introduction

Galaxy clusters form in the most massive dark matter halos that form in the Universe. With masses as large as $10^{14} h^{-1} M_{\odot}$, these dark matter halos are a result of the gravitational collapse of the highest density peaks in the initial density conditions that arise as a result of cosmic inflation (see e.g., Kaiser, 1984; Bardeen et al., 1986, see Kravtsov & Borgani 2012 for a recent review). Owing to their special location in the initial density field, the spatial distribution of these density peaks is biased compared to that of the matter distribution (Kaiser, 1984; Mo & White, 1996; Sheth et al., 2001; Tinker et al., 2010).

The amplitude of the spatial clustering of dark matter halos and hence the halo bias increases with halo mass. The dependence of halo bias on the mass has been theoretically predicted and measured using cosmological simulations. The clustering of various astrophysical objects such as galaxies or quasars is reflective of the clustering of dark matter halos which host them. Therefore the dependence of halo bias on halo mass is useful to infer the dark matter halo masses of these objects (Cooray & Sheth, 2002).

However, caution is warranted during any such inference of galaxy properties through their clustering. Although primarily dependent on halo mass, the halo bias could also depend on other secondary parameters correlated with halo assembly history (Gao et al., 2005; Gao & White, 2007). For example, Wechsler et al. (2006) demonstrated that at fixed halo mass, halo bias is also dependent upon the concentration of dark matter halos (see for example, Fig. 1 for a visual representation). Any such dependence of the halo bias on secondary parameters other than halo mass are called halo assembly bias. Halo assembly bias on galaxy cluster scales is related to the properties of the initial density peaks from which galaxy clusters form (Dalal et al., 2008). Thus far, most clustering measurements in the literature have been successfully fit with simple halo occupation distribution models without accounting for any halo assembly bias. This does not however rule out the presence of halo assembly bias (Zentner et al., 2014).

Numerical simulations predict that halo assembly bias should be largest for galaxy scale halos. Therefore there have been quite a few observational attempts to detect halo assembly bias (e.g., Yang et al., 2006; Tinker et al., 2012; Hearin et al., 2015). However, Lin et al. (2016), investigated the first of these claims and found contradicting conclusions based on the same data. There are two main lessons to be taken from the exercise of Lin et al. (2016). First, it is important to establish that the samples used for the observational detection of halo assembly bias are not contaminated with a population of satellite halos (i.e., some substructure of massive dark matter halos), and second, the two halos samples need to have the same halo mass, within the measurement uncertainties.

In what follows, I will review our recent attempts to detect halo assembly bias on galaxy cluster scales. The focus on galaxy cluster scales allows us to address both the lessons mentioned above. The contamination by satellite substructures in a galaxy cluster sample is expected to be small. The halo masses of galaxy clusters can be measured using the weak gravitational lensing signal. I will also then review some theoretical development of how the structure of dark matter halos can help unveil the current mass accretion rate to these halos (a quantity which should reflect the assembly history of halos), and report on the observational progress for the same.

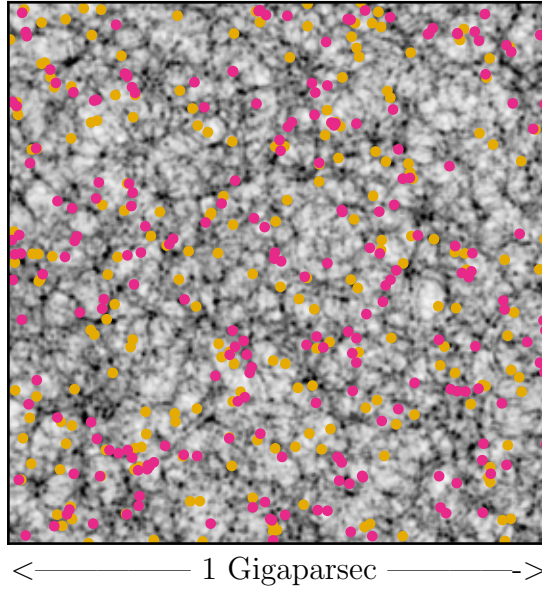


Figure 1: Halo assembly bias: The spatial distribution of two subsamples of cluster-sized dark matter halos from the collisionless numerical simulation - Multidark Planck (Klypin et al., 2016). These subsamples share the same mass distribution, but have different dark matter concentrations – the pink (yellow) halos have low (high) dark matter concentration parameters compared to the average given their halo mass. The halos depicted in pink are more clustered compared to those in yellow.

2. Galaxy cluster subsamples

We use the publicly available catalog of galaxy clusters identified from the SDSS DR8 photometric galaxy catalog by the *red*-sequence *Matched-filter Probabilistic Percolation* (redMaPPer) cluster finding algorithm (v5.10, see the website¹ for details and Rykoff et al., 2014; Rozo et al., 2015). The cluster finder identifies galaxy clusters as overdensities of red-sequence galaxies. The cluster catalog lists an estimate of the number of cluster galaxies, or optical richness λ , a photometric redshift estimate z_λ , as well as a most probable center for the galaxy cluster. A member galaxy catalog provides a list of members for each cluster, each of which is assigned a membership probability, p_{mem} .

We restrict ourselves to an approximately volume limited sample of 8,648 redMaPPer clusters with $20 < \lambda < 100$ and $0.1 \leq z_\lambda \leq 0.33$. The average redshift of our cluster subsamples is 0.24. This sample is subdivided into two based on the average projected cluster-centric separation of member galaxies as done in Miyatake et al. (2016). The samples are subdivided in such a manner that ensures that the two samples have the same optical richness distribution as well as redshift distribution, by construction. Each of these samples consist of 4,235 and 4,413 clusters, respectively.

For the measurement of the weak gravitational lensing signal, we made use of the weak lensing shape catalog of Reyes et al. (2012), which is based on the photometric galaxy catalog from the SDSS DR8. We also made use of the entire photometric galaxy catalog to measure the galaxy

¹<http://risa.stanford.edu/redmapper/>

cluster-galaxy cross-correlations for the purpose of detecting halo assembly bias, as reported in the next section.

3. Observational evidence for halo assembly bias

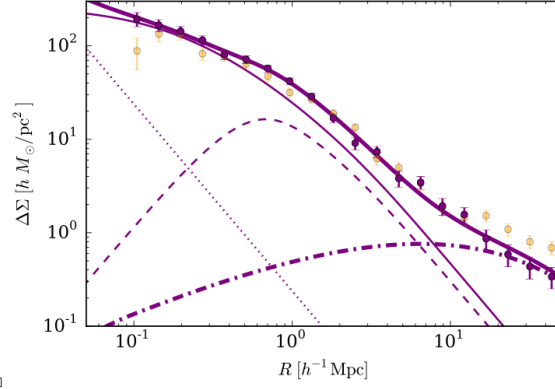


Figure 2: The purple and yellow data points with errorbars show the excess surface mass density profile as a function of the cluster-centric projected radius (in comoving units), obtained from the WL measurements for the large- and small- $\langle R_{\text{mem}} \rangle$ subsamples of redMaPPer clusters, respectively. This figure was adapted from (Miyatake et al., 2016).

In Miyatake et al. (2016), we presented the measurement of the stacked weak gravitational lensing signal of our two cluster subsamples (see Figure 2). The weak gravitational lensing signal for the two subsamples is remarkably similar in the inner regions (projected comoving radii $R < 10 h^{-1} \text{Mpc}$), while the signal for the two subsamples on scales beyond $15 h^{-1} \text{Mpc}$ differs by a factor 1.6. The weak lensing signal on small scales is sensitive to the halo mass and the halo density profile of the stacked galaxy clusters, while the large scale signal is sensitive to the halo bias of the two galaxy cluster subsamples. This qualitatively suggests that the two subsamples have the same mass, but a different large scale halo bias.

In Miyatake et al. (2016), we have presented a quantitative analysis of this weak lensing signal including a simple parametric model for the halo density profile. The results of this modelling indicate that both the cluster subsamples have a halo mass equal to $1.87 \times 10^{14} h^{-1} M_{\odot}$, with a statistical uncertainty of ~ 10 percent. The dark matter halo concentrations of the two subsamples are consistent with each other within the uncertainties, and yet the large scale halo bias of the two cluster subsamples is different by about 2.5σ .

The projected two point auto-correlation function of the galaxy cluster samples also confirms that the large scale bias of the two subsamples is indeed different. In Miyatake et al. (2016), we have also presented the ratio of the projected auto-correlation function of each of the subsamples to that of the parent sample which shows that the two subsamples should have large scale biases which are different with a significance of 4.6σ , and with values consistent with those obtained from the weak gravitational lensing signal.

In addition to these measurements, in More et al. (2016), we presented the ratio of the cross-correlation function of the cluster subsamples with the SDSS photometric galaxy samples (see

Fig. ??). This presents further confirmation that the halo bias of the two samples with equal masses are indeed different with a significance exceeding more than $5 - \sigma$. This measurement is a clear indication that halo clustering depends upon parameters other than the halo mass. If $\langle R_{\text{mem}} \rangle$ is related to the mass assembly history of halos, then this would be a clear indication of halo assembly bias.

In More et al. (2016), we have presented more systematic tests of projection effects and found that the projection effect could not significantly modify our conclusions about halo assembly bias.

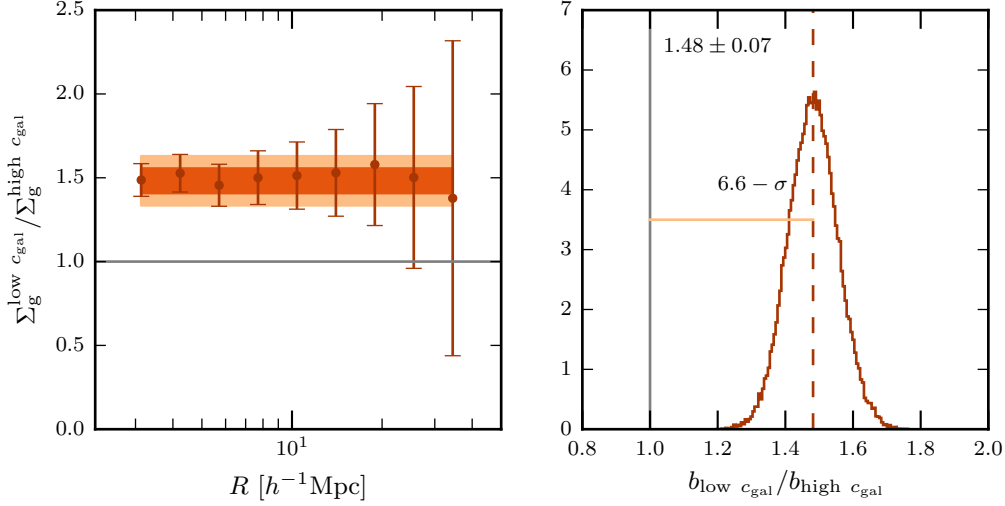


Figure 3: Halo assembly bias with cluster-galaxy cross-correlations. *Left panel:* The ratio of the surface number density profiles of our fiducial samples of photometric galaxies around the two galaxy cluster sub-samples. The shaded regions correspond to the 1- and 2-sigma confidence regions for a single constant parameter fit to these data. *Right panel:* The posterior distribution of the ratio given the measurements shown in the left panel. We detect halo assembly bias – difference in the halo biases of the two samples – at 6.6σ . There is a significant covariance in the errors, hence the small point-to-point variation given the errors. The quoted significance accounts for the covariance. This figure is taken from More et al. (2016).

4. The boundaries of dark matter halos

The inner structure of dark matter halos has been studied quite extensively using numerical simulations. In particular, the density profile of dark matter halos has received a lot of attention. These studies show that the density profile of dark matter halos is near universal, the so-called Navarro-Frenk-White profile, which asymptotes to -1 in the inner regions and -3 on large scales. This form of the density profile has been used as the de facto standard in order to interpret observational results as well.

In contrast, the issue of the boundary of dark matter halos has received relatively little attention. The boundaries of dark matter halos have been traditionally chosen to enclose an overdensity Δ with respect to some reference density. Common choices for boundaries include fixed values for Δ , for example, 200 with respect to the mean matter density, or $\Delta = 200, 500$ or even 2500 with respect to the critical matter density (see e.g. Tinker et al., 2010). Alternatively the virial overdensity

based on the spherical collapse model, where Δ changes with redshift has also been used (Bryan & Norman, 1998). Such varied definitions have the unintended consequence that the mass of the halo could grow even if the physical density of a dark matter halo stays constant (Diemer et al., 2013).

Do dark matter halos have definite physical boundaries? Recently, Diemer & Kravtsov (2014a), have argued that the outer density profiles of dark matter halos show a sharp steepening, much beyond that expected from the combination of the simple NFW profile and a large scale two halo term. They found that the location of this feature depends upon the mass accretion history of the halo. Using a simple analytical model of halo collapse, Adhikari et al. (2014) showed that this feature corresponds to the first apocenter of recently infalling material, and called it the splashback radius. This location corresponds to the last caustic in the secondary infall models of Fillmore & Goldreich (1984); Bertschinger (1985). In More et al. (2015), we have suggested that this splashback radius is a well motivated physical boundary of dark matter halos, as interior to the splashback radius, the infalling material starts to mix with material which has been at least once near the central regions of the halo.

The fact that the location of the splashback radius depends upon the mass accretion rate (Vogelsberger et al., 2011; Diemer & Kravtsov, 2014b; Adhikari et al., 2014) can also be very easily understood. Consider a dark matter particle falling down a potential well, and then climbing back up. If the potential well deepens during the infall of the particle, it reaches its apocenter at a radius which is smaller than where it started the infall from. The apocenter will be smaller for potential well which grow at a faster rate.

The splashback radius thus is a natural indicator of the accretion history of the halo.

5. Splashback radius in observations

In More et al. (2016), we measured the surface density distribution of photometric galaxies with absolute magnitudes ($M_i - 5 \log h < -19.43$) around the same cluster subsamples as those used to detect the halo assembly bias. In the left hand panel of Figure 4, we show the surface density distribution of galaxies around the two cluster subsamples. The logarithmic slope of the surface density profiles is shown in the right hand panel. It clearly shows that the location of the steepest slope is different for the two cluster subsamples, despite their similar weak lensing halo masses.

Does the steepest slope of the galaxy surface density profiles correspond to the splashback radius in observations? The steepest slope of the projected density profiles is at a location which is smaller than that of the three dimensional density profile. In More et al. (2016), we therefore presented a fit to the data using a parametric model for the three dimensional density profile. This allowed us to obtain the splashback radius for the two cluster subsamples. We find that the locations of the splashback radius for the two cluster subsamples are indeed different.

Our use of galaxy samples to infer the splashback radius also raises the question whether dynamical friction could affect the location of the splashback radius. Using subhalo abundance matching we estimate that the largest subhalos in which our galaxies reside is $V_{\text{peak}} > 135 \text{ km s}^{-1}$. Tests on numerical simulations show that subhalos with these V_{peak} in cluster scale halos splashback at a location which is not different by more than 5 percent than that of dark matter.

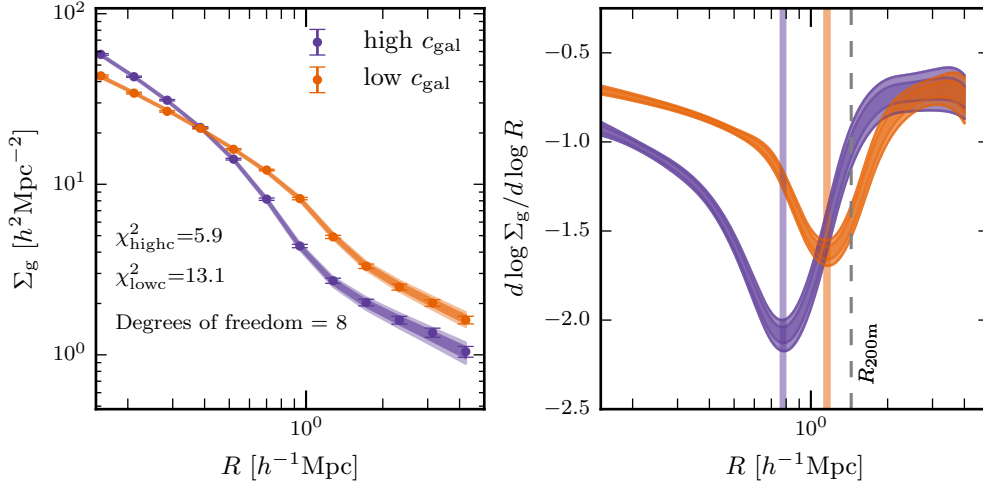


Figure 4: The surface number density profiles, $\Sigma_g(R)$, of our fiducial sample of SDSS photometric galaxies around the two cluster subsamples are shown in the left hand panel. The shaded regions show the 68 and 95 percent confidence regions of our model fit to the data. The right hand panel shows the inferred constraints on the logarithmic slope of $\Sigma_g(R)$ for the two subsamples. The splashback radius in 2d, R_{sp}^{2d} , corresponds to the location of the steepest slope or the minimum of $d \log \Sigma_g / d \log R$. The 68 percent constraints on R_{sp}^{2d} are marked with vertical shaded regions. These minima occur at significantly different locations for the two cluster subsamples. The traditional halo boundary, R_{200m} , is marked by the grey dotted vertical line.

6. Summary

We have used SDSS redMaPPer galaxy clusters and photometric galaxies around them to observationally investigate the boundaries of galaxy clusters, their relation to assembly history, and to halo assembly bias on galaxy cluster scales. In a series of papers in this topic, Miyatake et al. (2016) and More et al. (2016), we have thus been able to find two galaxy cluster subsamples which have the same average halo mass, different current mass accretion rates, and different large scale biases. This could be interpreted as a detection of halo assembly bias. Preliminary tests suggest that the level of halo assembly bias observed and the location of the splashback radius is discrepant with expectations from the standard structure formation model. Thorough tests on mock galaxy catalogs on which we could test our galaxy cluster sample selection can reveal whether these discrepancies are a result of various observational or cluster finding related systematics, or pointing to something more interesting about the Universe.

References

- Adhikari, S., Dalal, N., & Chamberlain, R. T. 2014, JCAP , 11, 19
- Bardeen, J. M., Bond, J. R., Kaiser, N., & Szalay, A. S. 1986, ApJ , 304, 15
- Bertschinger, E. 1985, ApJS , 58, 39
- Bryan, G. L., & Norman, M. L. 1998, ApJ , 495, 80

- Cooray, A., & Sheth, R. 2002, *Phys. Rep.* , 372, 1
- Dalal, N., White, M., Bond, J. R., & Shirokov, A. 2008, *ApJ* , 687, 12
- Diemer, B., & Kravtsov, A. V. 2014a, *ApJ* , 789, 1
- . 2014b, *ApJ* , 789, 1
- Diemer, B., More, S., & Kravtsov, A. V. 2013, *ApJ* , 766, 25
- Fillmore, J. A., & Goldreich, P. 1984, *ApJ* , 281, 1
- Gao, L., Springel, V., & White, S. D. M. 2005, *MNRAS* , 363, L66
- Gao, L., & White, S. D. M. 2007, *MNRAS* , 377, L5
- Hearin, A. P., Watson, D. F., & van den Bosch, F. C. 2015, *MNRAS* , 452, 1958
- Kaiser, N. 1984, *ApJ* , 284, L9
- Klypin, A., Yepes, G., Gottlöber, S., Prada, F., & Heß, S. 2016, *MNRAS* , 457, 4340
- Kravtsov, A. V., & Borgani, S. 2012, *ARA&A* , 50, 353
- Lin, Y.-T., Mandelbaum, R., Huang, Y.-H., Huang, H.-J., Dalal, N., Diemer, B., Jian, H.-Y., & Kravtsov, A. 2016, *ApJ* , 819, 119
- Miyatake, H., More, S., Takada, M., Spergel, D. N., Mandelbaum, R., Rykoff, E. S., & Rozo, E. 2016, *Physical Review Letters*, 116, 041301
- Mo, H. J., & White, S. D. M. 1996, *MNRAS* , 282, 347
- More, S., Diemer, B., & Kravtsov, A. V. 2015, *ApJ* , 810, 36
- More, S., et al. 2016, *ArXiv e-prints*
- Reyes, R., Mandelbaum, R., Gunn, J. E., Nakajima, R., Seljak, U., & Hirata, C. M. 2012, *MNRAS* , 425, 2610
- Rozo, E., Rykoff, E. S., Becker, M., Reddick, R. M., & Wechsler, R. H. 2015, *MNRAS* , 453, 38
- Rykoff, E. S., et al. 2014, *ApJ* , 785, 104
- Sheth, R. K., Mo, H. J., & Tormen, G. 2001, *MNRAS* , 323, 1
- Tinker, J. L., George, M. R., Leauthaud, A., Bundy, K., Finoguenov, A., Massey, R., Rhodes, J., & Wechsler, R. H. 2012, *ApJ* , 755, L5
- Tinker, J. L., Robertson, B. E., Kravtsov, A. V., Klypin, A., Warren, M. S., Yepes, G., & Gottlöber, S. 2010, *ApJ* , 724, 878
- Vogelsberger, M., Mohayaee, R., & White, S. D. M. 2011, *MNRAS* , 414, 3044

Wechsler, R. H., Zentner, A. R., Bullock, J. S., Kravtsov, A. V., & Allgood, B. 2006, *ApJ* , 652, 71

Yang, X., Mo, H. J., & van den Bosch, F. C. 2006, *ApJ* , 638, L55

Zentner, A. R., Hearin, A. P., & van den Bosch, F. C. 2014, *MNRAS* , 443, 3044